Observation-based Analysis of Ozone Production Sensitivity for Two Persistent Ozone Episodes in Guangdong, China

Kaixiang Song[1], Run Liu[1,2], Yu Wang[1,2], Tao Liu[1], Liyan Wei[1], Yanxing Wu[1], Junyu Zheng[1,2], Boguang Wang[1,2], Shaw Chen Liu[1,2]

[1]Institute for Environmental and Climate Research, Jinan University, Guangzhou, 511443, China
[2]Guangdong-Hongkong-Macau Joint Laboratory of Collaborative Innovation for Environmental Quality, Guangzhou, 511443, China

Correspondence to: Run Liu (liurun@jnu.edu.cn), Shaw Chen Liu (shawliu@jnu.edu.cn)

Abstract. An observation-based method (OBM) is developed to investigate the sensitivity of ozone formation to precursors during two persistent elevated ozone episodes observed at 77 stations in Guangdong. Average OH concentrations derived at the 77 stations between 08:00 and 13:00 local time stay within a narrow range of 2.5×10^6 cm^{-3} to 5.5×10^6 cm^{-3} with a weak dependence on the NOx. These values are in good agreement with OH values observed at a rural station in Pearl River Delta (PRD). They also agree well with a box model constrained by the ambient conditions observed during the two episodes. The OBM has been used to evaluate the ozone production efficiency, $\varepsilon(NO_x$ or VOC), defined as the number of O_3 molecules produced per molecule of NO_x (or VOC) oxidized. Average values of $\varepsilon(NO_x)$ and $\varepsilon(VOC)$ determined by the OBM are 3.0 and 2.1 ppb/ppb, respectively, both compared well with values in previous studies. Approximately 67% of the station-days exhibit ozone formation sensitivity to NO_x, approximately 20% of the station-days are in the transitional regime sensitive to both NO_x and VOC, only approximately 13% of the station-days are sensitive to VOC. These results are in semi-quantitative agreement with the ozone formation sensitivity calculated by the box model constrained by ambient conditions observed during the two episodes. However, our OBM results differ from those of most previous investigations which suggested that limiting the emission of VOC rather than NO_x would be more effective in reducing ozone reduction in Guangdong.

删除[liuru]: and a box model constrained by the ambient conditions

1 Introduction

Increases of surface ozone (O_3) can have serious adverse impacts on human health and ecological systems (Wang et al., 2005; Song et al., 2017; Lin et al., 2018). In addition, tropospheric ozone is a significant greenhouse gas (IPCC, 2013). With a high rate of urbanization and industrialization, and the increasing use of motor vehicles, Guangdong has been suffering from severe O_3 pollution (Zhang et al., 2011). The primary pollutant in Guangdong has switched from particle matters to O_3 since 2015, thanks to a stringent emission control policy that has effectively reduced other air pollutants (Department of Ecology and Environment of Guangdong Province, 2016). In fact, the number of days with O_3 as the primary pollutant is 68.7%, far exceeding that of $PM_{2.5}$ (15.8%) and PM_{10} (8.3%) in 2020 (Department of Ecology and Environment of Guangdong Province, 2021).

O$_3$ is a secondary pollutant produced from photochemical reactions involving nitrogen oxides (NO$_x$) and volatile organic compounds (VOCs) (Trainer et al., 2000; Zhang et al., 2014; Wang T. et al., 2017). Sensitivity of O$_3$ production is nonlinearly dependent on precursor concentrations, and is usually categorized into photochemical regimes such as NO$_x$-limited or VOC-limited (Kleinman et al., 1994; Sillman et al., 1998). There have been a number of studies on the sensitivity of O$_3$ production to NO$_x$ and VOC by photochemical air quality models (Sillman et al., 2003; Lei et al., 2004; Tang et al., 2010), as well as observation-based methods (OBM) (Thielmann et al., 2002; Zaveri et al., 2003; Shiu et al., 2007). Several modeling approaches have been used to evaluate the O$_3$ production sensitivity, including L$_N$/Q method, where L$_N$ is the radical loss via the reactions with NO$_x$ and Q is the total primary radical production (Kleinman et al., 2001; Kleinman, 2005; Mao et al., 2010), the relative incremental reactivity method (RIR) (Shao et al., 2009; Cheng et al., 2010; Lu et al., 2010a; Xue et al., 2014; Li et al., 2017) and the Empirical Kinetics Modeling Approach method (EKMA) (Dodge, 1977). These model-based studies usually have large uncertainties in their input parameters, particularly in the emission inventories and photochemistry of VOC (Chang et al., 2020). Observation-based methods can avoid some of the uncertainties by using observations to constrain the analysis (Thielmann et al., 2002; Zaveri et al., 2003; Shiu et al., 2007).

In this study, we adopt the approach proposed by Shiu et al. (2007) and develop an OBM to evaluate the O$_3$ production sensitivity during two multi-day O$_3$ pollution episodes in Guangdong. In this OBM, the concentration of OH is derived from observed NO$_x$ and CO in a new approach as described in the methodology section. The OBM is then used to evaluate the ozone production efficiency, ε(NO$_x$ or VOC), defined as the number of O$_3$ molecules produced per molecule of NO$_x$ (or VOC) oxidized. Finally, 3D-EKMA plots are generated basing on the OBM. The rest of the paper is organized as follows: Section 2 describes the data sources and analysis methods, Section 3 presents the results and discussions, and Section 4 presents a summary and conclusions.

2 Data and methodology

2.1 Data

Hourly surface O$_3$, PM$_{2.5}$, CO and NO$_2$ concentration data at 77 out of a total 102 stations in Guangdong operated by China National Environmental Monitoring Centre (CNEMC) during the period 2018–2019 are used in this study (available at http://www.cnemc.cn/en/). The 77 stations (Fig. 1a) are chosen for their completeness of data. It can be seen in Fig. 1a that polluted stations are mainly located in the PRD, while clean stations are located in the northeast of Guangdong. In this study, we choose two persistent O$_3$ pollution episodes to perform the OBM analysis, specifically October 2 to October 8, 2018 and September 24 to October 1, 2019. Figure 1b is the same as Fig. 1a except it shows the average ozone concentrations of all ozone exceeding days in Guangdong in 2018 and 2019. One can see clearly that the ozone distribution during the two episodes in autumn is representative of and even slightly higher than the ozone concentrations during ozone pollution days in Guangdong in the entire two years. In fact, the monthly peak ozone concentrations in Guangdong tend to occur in September

删除[liuru]: ure

and October because Guangdong is usually under heavily overcast conditions with southerly winds bringing clean moist air from the South China Sea in the summer which tends to suppress the ozone formation.

Hourly meteorological data are obtained from European Centre for Medium-Range Weather Forecasts ERA5 reanalysis, including relative humidity (RH), 2 m temperature (T), 10 m zonal wind (U10), 10 m meridional wind (V10), geopotential height, cloud cover, surface net solar radiation, boundary layer height and K-index, with a resolution of 0.25°×0.25° (available at https://www.ecmwf.int/).

2.2 Methods

2.2.1 Derivation of nitric oxide (NO) concentration

Since the observation of NO concentration ([NO]) is severely limited in CNEMC dataset, we calculate [NO] from the assumption of photochemical equilibrium between [NO_2] and [O_3] according to the following equation:

$$[NO] = \frac{J_{NO_2} \times [NO_2]}{[O_3] \times K_1} \tag{1}$$

where k_1 represents the reaction rate constant for the reaction of NO with O_3. This equation neglects the reactions of NO reactions with HO_2 and RO_2. The uncertainty due to this neglection is around 20%, which is acceptable as discussed in Section 3.5. The value of k_1 is taken from Seinfeld and Pandis (1998):

$$k_1(1/ppm/min) = 3.23 \times 10^3 \exp(-1430/T) \tag{2}$$

J_{NO_2} is the photolysis rate of NO_2. Its value depends on the solar zenith angle (χ) and total shortwave radiation (TSR) (Wiegand and Bofinger, 2000):

$$J_{NO_2} = \begin{cases} TSR \times \left[(4.23 \times 10^{-4}) + 1.09 \times \frac{10^{-4}}{\cos\chi}\right] & 0° \leq \chi \leq 47° \\ TSR \times (5.82 \times 10^{-4}) & 47° < \chi \leq 64° \\ TSR \times [(-0.997 \times 10^{-4}) + (1.2 \times 10^{-3}) \times (1 - \cos\chi)] & 64° < \chi \leq 90° \end{cases} \tag{3}$$

2.2.2 Derivation of VOC

In this study, we use CO as a tracer to estimate VOC. This tracer method has been widely used in previous studies (Heald et al., 2003; Hsu et al., 2010; Shao et al., 2011; Yao et al., 2012; Tang et al., 2013). Individual VOC at 08:00 are calculated by multiplying the freshly emitted CO at 08:00 with the ratio of VOC/CO in the emission inventories of Huang et al. (2021), according to the equations listed in the Supplementary Information. The freshly emitted CO is assumed to be the difference in CO between 08:00 and 13:00 as shown in Fig. 2 (Equation S1). The CO at 13:00 is considered to be the leftover CO for the following day, and is used to evaluate the leftover VOC (Equation S2). Oxidized VOC (OVOC) are estimated from the observed ratios of CH_2O, CH_3CHO and ketone to CO (Wang et al., 2016; Wu et al., 2020). Other OVOCs are not included. The VOCs and OVOCs derived this way can be validated by comparing with observed values in terms of the OH reactivity. Tan et al. (2019) reported that observed NOx, CO, HCHO and VOCs in PRD in autumn 2014 contributed, respectively, 14%, 10%, 5–8% and 20%, for a total of about 50% to the observed OH reactivity, which scale to 28%, 20%, 10–16% and 40%,

删除[fang]: warm moist

删除[fang]: the ocean

删除[fang]: are not conducive to

删除[fang]: (

删除[fang]:)

删除[liuru]: in turn

删除[liuru]: (

删除[liuru]: -

删除[liuru]:)

删除[liuru]: (

删除[liuru]: -

删除[liuru]:)

respectively when normalized to 100%. In comparison, in our study the average NOx, CO, OVOCs and VOCs contribute 33%, 17%, 24% and 26%, respectively to the OH reactivity. There is a reasonable agreement between our results and those of Tan et al. (2019) except for OVOCs and VOCs. The disagreement on OVOCs can be easily explained by the fact that HCHO accounts for about two thirds of the OVOCs in our case. Nevertheless, the underestimate of the VOC contribution in

95   our study remains unresolved and suggests significant uncertainty in the VOCs derived by our method.

删除[liuru]: our

2.2.3 Derivation of OH concentrations

The ratio ethylbenzene/m,p-xylene has been suggested to be a good measure of the photochemical processing by OH (Calvert, 1976; Singh, 1977; Shiu et al., 2007). Following a Lagrangian trajectory, the ratio can be shown as

$$E/X = (E_0/X_0)\exp\left(-\int_0^t (k_e-k_x)\,[OH]\,dt\right) \tag{4}$$

100   Where E and X represent concentrations of ethylbenzene and m,p-xylene at time t, respectively. E_0 and X_0 are their corresponding initial concentrations, k_x and k_e are their reaction rate constants with OH, k_x and k_e equal to 2.17×10^{-11} and 7.0×10^{-12} cm^3 s^{-1}, respectively (Atkinson, 1990). With known value of E_0/X_0, [OH×t] can be evaluated from observed E/X at time t. This provides an OBM derived density of OH.

In the real atmosphere, the Lagrangian condition rarely exists due to turbulence mixing as well as atmospheric advection.

105   Nevertheless, Equation (4) tends to hold because atmospheric transport affects the two species similarly. This is a key advantage of the OBM. In this study, due to limited measurements of VOC, we use CO and NO$_x$ to replace ethylbenzene and m,p-xylene, respectively.

删除[liuru]: E

删除[liuru]: X

2.2.4 Calculation of oxidized VOC and NOx

In this study, we consider reaction of NO$_2$ with OH as the only removal process for NO$_x$ and assume the removal of NO$_x$ is

110   pseudo-first order as shown below. In this case, following the Lagrangian trajectory, we have:

$$[NO_x]=[NO_x]_0\exp\left(-k\int_0^t [OH]\,dt\right) \tag{5}$$

where k is the reaction rate constant of NO$_x$ with OH. The reaction rate constant for NO$_2$ and OH is 1.04×10^{-11} cm^3 s^{-1} at 25 ^{o}C and 1 atm pressure according to Sander et al. (2003). Since NO$_2$ is part of NO$_x$, the value of k should be scaled down by the ratio NO$_2$/NO$_x$. The average of NO$_2$/NO$_x$ ratio is about 0.6, thus k for NO$_x$ is prescribed at 6.0×10^{-12} cm^3 s^{-1}.

115   Similarly, we have:

$$[VOC_s]=[VOC_s]_0\exp\left(-k_{vocs}\int_0^t [OH]\,dt\right) \tag{6}$$

$$[CO]=[CO]_0\exp\left(-k_{co}\int_0^t [OH]\,dt\right) \tag{7}$$

where k_{voc} and k_{co} are the reaction rate constants of VOCs and CO with OH, respectively. K_{VOC} of individual VOC are listed in Table S1 and k_{co} is prescribed at 1.4×10^{-13} cm^3 s^{-1} (Atkinson et al., 2006).

删除[liuru]: k_{CO}

Since the Lagrangian condition is sometimes not observed, it is necessary to select the time periods during which the quasi-Lagrangian condition as shown in Fig. 2 is valid approximately. The selection criterion is that the ratio of CO concentrations between 08:00 and 13:00 lies within 50% of 1-standard deviation (vertical bars) of the ratio of CO shown in Fig. 2 which is assumed to be in the Lagrangian condition. This criterion usually filters out about 60% of data, i.e., about 40% of the days satisfy approximately the Lagrangian condition. We have tested this selection criterion by parameterizing it between 30% to 80% of 1-standard deviation and found our major results are robust within this range.

删除[liuru]: one half

2.2.5 Dilution effect

Diurnal variations of pollutants averaged over all stations and the two episodes are shown in Fig. 2. Previous studies have shown that part of the early morning rise in O_3 is due to O_3 entrained from the residual layer above the boundary layer during the development of the boundary layer in the morning (Shiu et al., 2007; Zhao et al., 2019). We adopt the approach proposed by Shiu et al. (2007) to account for the dilution effects. Specifically, the reduction of CO concentrations from 08:00 to 13:00 (approximately 20%) is assumed to be the dilution effect, and used for all other species. The uncertainty due to this assumption is discussed in section 3.5.

2.2.6 Emissions of NOx, CO and VOC between 08:00 and 13:00

Equations (5), (6) and (7) do not account for the emissions of NO_x, CO or VOC during the period of 08:00–13:00. Inclusion of these emissions would affect the value of OH derived from Equation (5) as well as the dilution effect. We estimate the emission of NO_x by taking advantage of the fact that NO_x reaching a quasi-steady state around 13:00–16:00 as evident in Fig. 2. We believe that the quasi-steady state is maintained by the balance between the oxidation of NO_x and its emission. This is based on the notion that oxidation of NO2 by OH is the predominant sink of NOx in 13:00–16:00, of which the integration over the mixed/boundary layer should be balanced by the emission flux of NOx according to the continuous equation of NOx. Assuming the oxidation loss rate of NOx in the mixed layer is uniform with height, we obtain that the divergence of the hourly NOx emission rate is equal to the oxidation loss rate of NOx in 13:00–16:00. Using the average OH of 5×10^6 cm^{-3} at noontime derived from Equation (5) (Fig. 4) and mean NO_x in 13:00–16:00 (Fig. 2), a value of approximately 1.8 ppb per hour can be obtained. This value is assumed to be the hourly NOx emission rate between 08:00 and 13:00. The emissions of CO and VOC are calculated using their ratios to NO_x in the emission inventories of Huang et al. (2021).

删除[fang]: increase

删除[Liu Emma]: 5

2.2.7 Box model

A photochemical box model with carbon bond mechanism (PBM-CB05) (Yarwood et al., 2005; Coates and Butler, 2015; Wang Y. et al., 2017) is used to simulate the O_3 production rate and OH radical. Unlike emission-based models, the PBM-CB05 used in this study is based on observed concentrations of air pollutants and meteorological parameters (Wang Y. et al., 2017). In the CB05 module, VOCs are grouped according to carbon bond type and the reactions of individual VOCs are condensed using the lumped structure technique (Yarwood et al., 2005; Coates and Butler, 2015). In this study, the pollution

indicators (O₃, NO, NO₂, CO and VOC) and meteorological parameters (temperature, relative humidity, pressure) observed during the two episodes are utilized as input parameters for the model. There are 37 VOC species considered in our case. The model simulation starts from 07:00 and end at 18:00 with hourly input data based on observed concentrations of air pollutants and meteorological parameters during the two episodes.

3 Results and discussion

3.1 Air quality and meteorological conditions

Figure 3 shows the time series of hourly concentrations of air pollutants. The time period covers the two ozone episodes and extends to two days before and two days after. Mean maximum daily 8-h average (MDA8) O_3 concentrations in the episode1 was 88.7 ppb, and the episode2 was 99.6 ppb. The average daily concentration of CO of the two episodes was 0.74 and 0.85 ppm, respectively. The corresponding time series of key meteorological parameters are shown in Fig. S1. As O_3 is formed through photochemical reactions involving precursors NO_x and VOC, strong solar radiation, high temperature and low wind speed have been identified to be common conditions conducive to the formation of ozone (Liu et al., 2017; Wang L. et al., 2018). During both O_3 episodes, the weather in Guangdong was dominated by high pressure systems with warm and cloudless conditions, and northeasterly winds. In particular, the average maximum temperature for the episode1 was 28℃ and the episode2 was 30℃.

The general patterns of O_3 concentrations of the two episodes were similar. Relatively high O_3 concentrations with northerly or northeasterly winds appeared at least two days before the episode in both episodes. Afterward, the high O_3 kept increasing or stayed at a high level until the prevailing northeasterly wind shifted away and the surface pressure dropped. Starting on September 22, 2018, a precipitation event occurred which obviously ended the first episode. The heavier cloud cover greatly reduced the intensity of solar radiation and O_3 photochemical formation reactions. The disappearance of high O_3 in the second episode is believed to be related to a shift to southerly winds that brought in clean moist air from the South China Sea.

3.2 OH concentrations derived from OBM

Figure 4 shows the hourly OH concentrations between 08:00 and 13:00 derived from Equation (4) based on the concentrations of NO_x and CO observed at the 77 stations. Average OH concentrations derived at the 77 stations between 08:00 and 13:00 local time stay within a narrow range of $2.5×10^6$ cm^{-3} to $5.5×10^6$ cm^{-3} with a weak dependence on the NOx. The mean OH concentrations and their 1-standard deviations derived by the OBM (black dots and black vertical bars, respectively) are approximately 30% higher than the mean OH concentrations and 1-standard deviations observed at a rural station in PRD in October–November 2014 (blue line and blue shade, respectively) (Tan et al., 2019). Nevertheless, there is a complete overlap of the 1-standard deviations of the two data sets (blue shade and black vertical bars), which indicates a good agreement between our OBM OH values and those observed by Tan et al. (2019). In another comparison with a previous investigation, our OH concentrations are approximately 40% lower than the OH calculated by a box model

删除[Liu Emma]: 4

删除[fang]: warm

删除[fang]: and

删除[Liu Emma]: 5

删除[fang]: nearly

constrained by observed air pollutants during an experiment at a remote island site in the PRD from August to November 2013 (red line and red shade) (Wang Y. et al., 2018). There is also a nearly complete overlap of the 1-standard deviations of the two data sets (red shade and black vertical bars). Figure 4 also includes the noontime OH concentrations calculated by the box model described above. The box model is constrained by the ambient conditions observed during the two episodes. The average modelled OH concentration is approximately 3.2×10^6 cm^{-3} with a 1-standard deviation of 0.6×10^6 cm^{-3} (red cross and red vertical bar, respectively). This value of OH is approximately 40% less than the OH values of $5.5\pm4.3\times10^6$ cm^{-3} derived by the OBM at noontime. Again, there is a good overlap of the 1-standard deviations of the two data sets. The agreement among the OH concentrations derived by the OBM, the box model and field observations gives credence to our observation-based analysis, at least in terms of the derived OH concentration which plays a critical role in the O$_3$ formation. Nevertheless, we acknowledge that the OH concentrations derived here are approximately a factor of 3 to 5 lower than the OH concentrations observed at Backgarden (a suburban site about 70 km downwind of Guangzhou) during an intensive campaign in 2006, in which the OH reached daily peak values of $15–26\times10^6$ cm^{-3} (Lu et al., 2012). This discrepancy remains unresolved.

3.3 Ozone production efficiency

Ozone production efficiency (ε) is defined as the number of O$_3$ molecules produced per molecule of NO$_x$ (or VOC) oxidized photochemically (Liu et al., 1987; Trainer et al., 2000). ε can be calculated by the following equations:

$$\varepsilon[NOx] = \Delta[O_3]/\Delta[NO_x]$$

$$\varepsilon[VOC] = \Delta[O_3]/\Delta[VOC]$$

where $\Delta[O_3]$ represents the amount of ozone generated from 08:00 to 13:00 which is equal to the observed difference in O$_3$ between 08:00 and 13:00, after adjustment to the dilution factor. $\Delta[NO_x]$ ($\Delta[VOC]$) represents the consumption/oxidation of NO$_x$ (VOC) between 08:00 and 13:00.

Figure 5a shows the relationship of ε as a function of the average NO$_x$ concentration between 08:00 and 13:00. As expected ε is greater at lower NO$_x$, i.e., the O$_3$ production efficiency is greater in rural and suburban environments than urban conditions, in agreement with previous findings (Liu et al., 1987; Kleinman et al., 2002). The value of $\varepsilon(NO_x)$ converges to a narrow range of about 1.0 ± 0.5 when NO$_x$ is greater than 70 ppb. This range of $\varepsilon(NO_x)$ in Fig. 5a is consistent with previous investigations in urban environments (Sillman et al., 1998; Daum et al., 2000) as well as in rural environments (Chin et al., 1994; Trainer et al., 1995). Compare to previous investigations in PRD areas, values in Fig. 5a at NOx higher than 20 ppb are in good agreement with the $\varepsilon(NOx)$ values of 2.1–2.5 found at urban stations in PRD by Yu et al. (2020) and Lu et al. (2010b). However, $\varepsilon(NOx)$ values of 6.0–13.3 were found at rural stations in PRD (Lu et al., 2010b; Wei et al., 2012; Xu et al., 2015; Yang et al., 2017), which are about a factor of 2 higher than our values at low NOx. Considering that our values are derived for two ozone pollution episodes in which the $\varepsilon(NOx)$ should be higher than non-episode periods, this discrepancy is puzzling. Figure 5b is the same as Fig. 5a except that the x-axis is changed to $\Delta[NO_x]$ or the oxidized NO$_x$. Fig. 5b shows a relatively smoother distribution compared to Fig. 5a, most likely because that the oxidized NO$_x$, rather than

NO$_x$ itself, is more closely related photochemically to Δ[O$_3$]. As Δ[NO$_x$] increases beyond 30 ppb, ε[NO$_x$] levels off linearly to a nearly constant value around 1.0 when Δ[NO$_x$] approaches 80 ppb (Fig. 5b). ε[VOC] is also greater at lower Δ[VOC], and has an asymptotic value of about 1.0±0.5 when Δ[VOC] gets greater than 50 ppb (Fig. 5c).

Figures 5b and 5c have some useful implications for the ozone control strategy. For instance, ε[NO$_x$] = 1.7 when Δ[NO$_x$] = 50 ppb can be interpreted as - in a highly polluted ambient environment in Guangdong where Δ[NO$_x$] equals 50 ppb, approximately 1.7 ppb of ozone is produced for each ppb of NO$_x$ oxidized. The overall average value of ε[NO$_x$] is about 3.0 (Fig. 5b), which implies in average 3.0 ozone molecules are produced for each NO$_x$ molecule oxidized. The overall average value of ε[VOC] is approximately 2.1 (Fig. 5c), which implies 2.1 ozone molecules are produced for each VOC molecule oxidized, about 50% less efficient than that of NO$_x$.

Photochemical oxidation of a VOC molecule under common ambient urban conditions produces approximately two or more peroxyl radicals–one HO$_2$ and more than one RO$_2$ (Seinfeld and Pandis, 1998; Jacob, 1999). Because there is abundant NO$_x$ in the ambient atmosphere in Guangdong, nearly all peroxyl radicals are expected to react with NO to produce NO$_2$ and then O$_3$. Jacob (1999) suggested an ozone formation rate of 2Δ[VOC] in the urban atmosphere. This is in excellent agreement with the overall value of 2.1Δ[VOC] found here by the OBM. This agreement as well as the consistency with previous investigations on the ε[NO$_x$], provides credence again to the observation-based analysis of this study.

3.4 Ozone sensitivity to precursors

The sensitivity of ozone formation (ΔO$_3$) to ozone precursor NO$_x$ is examined in Fig. 6a in which ΔO$_3$ (right hand side in red) and the oxidized VOC (left hand side in black) are plotted as a function of the oxidized NO$_x$. Similarly in Fig. 6b ΔO$_3$ (right hand side in red) and the oxidized NO$_x$ (left hand side in black) are plotted as a function of the oxidized VOC. It can be seen in Fig. 6a that ΔO$_3$ increases with the value of oxidized NO$_x$. The increase first has a very sharp slope of about 2.0 ppb/ppb when oxidized NO$_x$ is below 30 ppb, indicating a strong sensitivity of ozone formation to oxidized NO$_x$. The slope flattens out quickly to around 0.2 ppb/ppb when oxidized NO$_x$ gets greater than 30 ppb, suggesting other factors such as VOC and the VOC/NO$_x$ ratio may become more important in controlling the ozone formation rate. Fig. 6b shows that ΔO$_3$ increases with the value of oxidized VOC with a slope of about 0.4 ppb/ppb. However, this slope is much smaller than that of NO$_x$, especially in the low oxidized NOx regime (<30 ppb). In a brief summary for Figs. 6a and 6b, the ozone formation is most sensitive to the oxidized NO$_x$ in relative clean regimes of oxidized NO$_x$<30 ppb. In more polluted regimes, other factors such as the initial VOC and/or the VOC/NO$_x$ ratio appear to have a significant impact on the ozone formation. Additional evidence in support of these points is elaborated below.

Figure S2 presents a three-dimensional EKMA-like depiction of ozone formation rates (ΔO$_3$, black dots, 471 points) plotted as a function of the oxidized NO$_x$ (x-axis) and oxidized (VOCs+CO) (y-axis). The colored plane is a linear regression to the ozone formation rates (black dots), and the green and red bars denote positive and negative deviations of individual dots from the plane, respectively. Different color shades from blue to red denote different concentrations of ΔO$_3$ in ppb. The equation for [ΔO$_3$] represents the plane as a function of the oxidized NO$_x$ (ΔNO$_x$) and oxidized VOC (ΔVOC). The

coefficients in front of ΔNO_x and ΔVOC in the equation are the ozone sensitivities to ΔNO_x and ΔVOC, respectively. The plane fits the black dots (ozone formation rates) reasonably well with an R^2 value of 0.423. The coefficient of ΔNO_x is 0.755 which is about 3 times of that of ΔVOC (0.247), indicating the ozone formation rate is about 3 times more sensitive to ΔNO_x than ΔVOC when consider all data at the 77 stations in Guangdong during the two episodes. This is consistent with the findings from Figs. 6a and 6b.

There appear some uneven congregations of red and green bars, e.g., a large number of red bars have low values of ΔNO_x, while many green bars tend to have moderate values of ΔNO_x and high values of ΔVOC. This suggests that there is a need to divide Fig. S2 into different congregations/regimes. Figure 7 is the same as Fig. S2 except dividing it into four quadrants of different levels of oxidized ozone precursors: Quadrant (a) low ΔNO_x and low ΔVOC (ΔNO_x<20 ppb, ΔVOC<25 ppb), Quadrant (b) high ΔNO_x and high ΔVOC (ΔNO_x>20 ppb, ΔVOC>25 ppb), Quadrant (c) low ΔNO_x and high ΔVOC (ΔNO_x<20 ppb, ΔVOC>25 ppb), Quadrant (d) high ΔNO_x and low ΔVOC (ΔNO_x>20 ppb, ΔVOC<25 ppb).

39% of all data points (184 out of 471 points) lie in Quadrant (a), the slope of ΔO_3 against ΔNO_x (coefficient of ΔNO_x in the equation) is approximately 1.54 ppb/ppb (p value < 0.01), while the slope of ΔO_3 against ΔVOC (coefficient of ΔVOC) has a value of 0.28 ppb/ppb (p value = 0.021). These values of slopes imply that the ozone formation at stations in Quadrant (a), a relatively clean environment, is about five times more sensitive to ΔNO_x than ΔVOC, i.e. the ozone formation is NO_x-limited. This is in good agreement with the conclusion reached based on Figs. 6a, 6b and S2. Quadrant (b) contains about 20% of the data points. The coefficient of ΔNO_x is 0.3 ppb/ppb (p value < 0.01), while the coefficient of ΔVOC is 0.29 ppb/ppb (p value = 0.043), suggesting that the ozone formation is sensitive to both ΔVOC and ΔNO_x. This quadrant belongs to the transitional regime. Quadrant (c) has 28% of the data points, the coefficients of ΔNO_x and ΔVOC are 2.25 ppb/ppb (p value < 0.01) and 0.04 ppb/ppb (p value = 0.785), respectively. Here again the ozone formation is NO_x-limited. Quadrant (d) has 13% of the data points, the coefficients of ΔNO_x and ΔVOC are 0.18 ppb/ppb (p value = 0.126) and 0.91 ppb/ppb (p value = 0.037), respectively. These values of coefficients indicate that the ozone formation is more sensitive to ΔVOC than ΔNO_x, i.e. the ozone formation is VOC-limited.

The analysis above provides an observation-based method for evaluating the ozone-precursor sensitivity. This method has the potential to provide quantitative information on the ozone control strategy for individual regions. In theory, the quadrants can be further divided into, for example, a specific region represented by individual stations, such that an ozone control strategy suitable to the region could be developed. In practice, this is limited by the data available for making the 3-dimentional plot like Fig. 7.

We have compared the OBM results to those of the box model constrained by the observed ambient environment in this study. Figure 8 shows the traditional 2D-EKMA plot calculated by the model. To facilitate the comparison, the x-axis and y-axis in Fig. 8 are changed to hourly oxidized NO_x and oxidized VOC, respectively, rather than the usual early morning concentrations of NO_x and VOC. The modeled results are shown in colored isopleths of ozone increments between 06:00 and 16:00 local time, while results of the OBM are shown in colored dots for ozone increment/formation between 08:00 and 13:00. The difference in the length of time has negligible effect on the ozone increment as evident in Fig. 2. The OBM

values agree with the model results semi-quantitatively. For instance, the colored dots of OBM shift from blue (20 ppb) to green (60–80 ppb) consistently with the colored isopleths, but the OBM dots rarely turn yellow when modeled isopleths get greater than 90 ppb. Two red lines (left-red and right-red) are added to Fig. 8 to facilitate the assessment of the sensitivity of ozone formation. There are 127 points located to the left of left-red line, which clearly belongs to the NO_x-limited regime according to the modeled ozone isopleths. There are 141 points located to the right of right-red line, which clearly belongs to the VOC-limited regime according to the modeled ozone isopleths. In between the two red lines contains 203 points, which are in the transitional regime sensitive to both NO_x and VOC. These three regimes overlap and agree in ozone formation sensitivity with Quadrants (a and c), Quadrant (d) and Quadrant (b) of the OBM results, respectively. However, the numbers of points in the three regimes deviate significantly from those of four OBM Quadrants. For example, Quadrant (b) has only 97 points compared to the 203 points in the transitional regime of Fig. 8; Quadrant (d) has only 60 points compared to the 141 points in the VOC-limited regime of Fig. 8; while Quadrants (a and c) has 314 points compared to the 127 points in in NO_x-limited regime of Fig. 8. In terms of ozone sensitivity, the modeled results show nearly equal number of points in the NO_x-limited regime as the VOC-limited regime, while the OBM results show five to one in favor of the NO_x-limited regime. A quantitative agreement between the OBM results (dots) and the modeling results (isopleths) would require to shift the dots in Fig. 8 leftward by approximately 0.5–1 ppbv h^{-1}, which would mean a reduction of OH by approximately 30–50%. Interestingly this requirement matches well with the fact that modeled OH is approximately 40% less than the OH value derived by the OBM at noontime as shown in Fig. 4.

Comparing with previous studies, we notice that almost all previous researches suggested that limiting the emission of VOCs in Guangdong would have a positive role in reducing ozone reduction (Zhang et al., 2008; Wang T. et al., 2017; Jiang et al., 2018), but different results may appear in different places and time. Yu et al. (2020) found that NO_x reduction in Shenzhen has led to higher ozone production from 2015 to 2018 given the nearly constant VOC. However, the ozone mitigation would be benefit from further NO_x reduction under the conditions of 2018. Yang et al. (2019) analyzed the relationship between ozone and precursors in PRD from 2007 to 2017 and found that the northeastern PRD was NO_x-limited and the southwest VOC-limited. Obviously, these findings are in general different from our results except in highly polluted environment like Quadrant (b). Some of the difference can be explained by the fact that most of the previous studies were focused on urban regions, while many rural stations are included in our OBM analysis. Finally, we acknowledge that our results are based on the analysis of only two multi-day ozone episodes which maybe not representative of the general ambient environment in Guangdong. A comprehensive regional and temporal OBM analysis is needed to make a definitive comparison with previous findings.

In summary of Section 3.4, the sensitivity of ozone formation to its precursors is complex and highly dependent on the ambient conditions of the station-day. Our OBM shows that approximately 67% of the station-days exhibit ozone formation sensitivity to NO_x, approximately 20% of the station-days are in the transitional regime sensitive to both NO_x and VOC; only approximately 13% of the station-days are sensitive to VOC. These findings are different from results of most previous studies, which favor ozone formation sensitivity to VOC.

删除[Liu Emma]: 10

删除[Liu Emma]: 10

删除[Liu Emma]: 10

删除[Liu Emma]: 10

删除[Liu Emma]: 10

删除[Liu Emma]: 5

3.5 Uncertainty analysis

315 Significant uncertainties and limitations exist in our OBM analysis. First and foremost is the uncertainty involved with the Lagrangian air mass assumption, which doesn't take into account of mixing, entrainment or surface deposition effects. Omitting the mixing of NO_x emitted between 08:00 and 13:00 into the Lagrangian air mass can lead to an underestimate of the OH concentration, while omitting the mixing of CO emission can underestimate the dilution effect. We account for the mixing of NO_x emission by assuming that NO_x reached a quasi-steady state around 13:00–16:00 (Section 2.2.6), and in turn

320 the mixing of CO and VOC emissions are calculated using their ratios to NO_x in the emission inventories of Huang et al. (2021). However, no surface deposition effect is included. The selection criterion defined by 50% of 1-standard deviation $(1.0\pm0.5\sigma)$ from the mean CO distribution works well in filtering out those data deviating significantly from the Lagrangian condition. However, the criterion filters out about 60% of the data, thus limiting the representativeness of the OBM analysis. This limitation has been evaluated by relaxing the selection criterion to $1.0\pm0.8\sigma$, which filters out only about 30% of the

325 data. No significant difference has been detected, suggesting the results of the OBM analysis are representative of the majority of the data. Another source of uncertainty is that one single dilution factor is adopted for all air pollutants, including O_3, CO, $PM_{2.5}$ and NO_x. In this context, it is reassuring to find out that the dilution factor derived independently from CO and $PM_{2.5}$ agrees within 10% with each other. In a brief summary, we estimate the uncertainty involved with the Lagrangian assumption to be in the range of 20–40%.

330 The second largest source of uncertainty is the evaluation of VOCs. Individual VOCs, including OVOCs, are calculated based on the observed concentration of CO and the ratio of VOC/CO in the emission inventories as discussed in Section 2.2.2. We have evaluated the VOCs and OVOCs derived this way by comparing their contributions to the OH reactivity observed by Tan et al. (2019) in PRD in autumn 2014. There is a reasonable agreement between our estimates of the contributions of NOx, CO, OVOCs and VOCs to the OH reactivity and those of Tan et al. (2019) except for a 35%

335 underestimation of VOCs. Hence we estimate the uncertainty in the evaluation of VOCs to be in the range of 30–50%. Another source of uncertainty may come from the neglection of heterogeneous reactions in this study. The largest impact of neglecting heterogeneous reactions is most likely to involve NOx between 08:00 and 13:00, during which the OH is derived. Since the effect of heterogeneous reactions is included in the observations, the neglect of any heterogeneous removal of NOx (e.g. deposition of NOx on aerosols in the humid conditions in Guangdong) can lead to an overestimate of OH

340 concentrations by the OBM. This would have a significant impact on the outcome of this study, as OH plays a critical role in the photochemistry of NOx, VOCs and ozone. On the other hand, presence of significant natural sources of NOx such as biogenic emission and/or lightning source in 08:00–13:00 would lead to an underestimate of OH concentration.

Finally, another source of uncertainty is attributable to the coarse resolution of CO measurements which is reported at 0.1 ppm intervals. As a result, many hourly CO data would show identical values and lose its value as a tracer.

删除[liuru]: s

删除[liuru]: -

删除[Liu Emma]: Individual VOCs at 08:00 are calculated by multiplying the fresh emission of CO at 08:00 with the ratio of VOC/CO in the emission inventories (Huang et al., 2021). The fresh emitted CO is assumed to be the difference in CO between 08:00 and 13:00. The CO at 13:00 is considered to be the leftover CO for the following day, and is in turn used to evaluate the leftover VOC. Oxidized VOC or OVOC are estimated from the observed ratios of CH2O, CH3CHO and ketone to CO (Wang et al., 2016). No other OVOC is included.

设置格式[liuru]: 英语(美国)

设置格式[liuru]: 英语(美国)

设置格式[liuru]: 英语(美国)

删除[fang]: PRD

设置格式[liuru]: 英语(美国)

删除[fang]: -

设置格式[liuru]: 英语(美国)

设置格式[liuru]: 英语(美国)

设置格式[liuru]: 英语(美国)

删除[liuru]: A

删除[liuru]: We estimate the uncertainty in the evaluation of VOCs to be in the range of 30%.

4 Summary and Conclusions

In this study, two persistent elevated ozone episodes in Guangdong (77 stations) that occurred in October 2–October 8, 2018 and September 24–October 1, 2019 were analyzed to investigate the sensitivity of ozone generation to precursor concentrations at the 77 stations. An OBM is developed by modifying the approach suggested by Shiu et al. (2007). Specifically, NO_x and CO are used in this OBM to substitute for the two hydrocarbon species utilized in Shiu et al. (2007). Major outputs from the OBM include the OH concentrations, O_3 production efficiency and the sensitivity of ozone formation to the precursors at the 77 stations during the two ozone episodes. The average OH concentrations between 08:00 and 13:00 agree well with the OH values observed at a rural station in PRD in October–November 2014 by Tan et al. (2019). The OH values derived from the OBM are also in good agreement with a box model constrained by the ambient conditions observed during the two episodes. On the other hand, the OH concentrations derived here are approximately a factor of 2 to 4 lower than the OH concentrations observed at Backgarden, a suburban site about 70 km downwind of Guangzhou (Lu et al., 2012). The O_3 production efficiency against NO_x, $\varepsilon(NO_x) = \Delta[O_3]/\Delta[NO_x]$, is greater at lower NO_x (Fig. 5a), in agreement with previous findings (Liu et al., 1987; Kleinman et al., 2002). The value of ε converges to a narrow range of about 1.0 ± 0.5 when NO_x is greater than 70 ppb. This range of $\varepsilon(NO_x)$ is consistent with previous investigations in urban environments (Sillman et al., 1998; Daum et al., 2000) as well as in rural environments (Chin et al., 1994; Trainer et al., 1995). Compare to previous investigations in PRD areas, our values of $\varepsilon(NO_x)$ at NOx higher than 20 ppb are in good agreement with the values of 2.1–2.5 found at urban stations in PRD by Yu et al. (2020) and Lu et al. (2010b). However, $\varepsilon(NO_x)$ values of 6.0–13.3 were found at rural stations in PRD (Lu et al., 2010b; Wei et al., 2012; Xu et al., 2015; Yang et al., 2017), which are about a factor of 2 higher than our values at low NOx. Considering that our values are derived for two ozone pollution episodes in which the $\varepsilon(NO_x)$ should be higher than non-episode periods, this discrepancy is puzzling. The overall average value of $\varepsilon[NO_x]$ is about 3.0 (Fig. 5b), which implies on average three ozone molecules are produced for each NO_x molecule oxidized. The overall average value of $\varepsilon[VOC]$ is approximately 2.1 (Fig. 5c), which implies 2.1 ozone molecules are produced for each VOC molecule oxidized, about 50% less efficient than that of NO_x. Jacob (1999) suggested an ozone formation rate of $2\Delta[VOC]$ in the urban atmosphere. This is in excellent agreement with the value of $2.1\Delta[VOC]$ found here by the OBM. This agreement as well as the consistency with previous investigations on the $\varepsilon[NO_x]$ and OH concentrations, provide credence to the observation-based analysis (OBM) of this study.

The sensitivity of ozone formation to its precursors is complex and highly dependent on the ambient conditions of the station-day. Our OBM shows that approximately 67% of the station-days exhibit ozone formation sensitivity to NO_x, approximately 20% of the station-days are in the transitional regime sensitive to both NO_x and VOC, only approximately 13% of the station-days are sensitive to VOC. These findings are different from results of most previous studies, which favor ozone formation sensitivity to VOC. Some of the difference can be explained by the fact that most of the previous studies were focused on urban regions, while many rural stations are included in our OBM analysis. Finally, we acknowledge that our results are based on the analysis of only two multi-day ozone episodes which maybe not representative of the general

删除[Liu Emma]: 6a

删除[fang]: three

删除[Liu Emma]: 6b

删除[Liu Emma]: 6c

ambient environment in Guangdong. A comprehensive spatial and temporal OBM analysis is needed to make a definitive comparison with previous findings.

380

Data availability. Hourly surface O_3, $PM_{2.5}$, CO and NO_2 data were obtained from China National Environmental Centre (http://www.cnemc.cn/en/, last access: 10 November 2021). Hourly meteorological data are obtained from European Centre for Medium-Range Weather Forecasts ERA5 reanalysis (https://www.ecmwf.int/, last access: 10 November 2021). The data of this paper are available upon request to Shaw Chen Liu (shawliu@jnu.edu.cn).

385

Author Contributions. SL proposed the essential research idea. KS performed the analysis. KS, RL and SL drafted the manuscript. YW, TL, LW, YW, JZ, and BW helped analysis and offered valuable comments. All authors have read and agreed to the published version of the manuscript.

390 *Competing interests.* The authors declare that they have no conflict of interest.

Acknowledgments. The authors thank the China National Environmental Centre and European Centre for Medium-Range Weather Forecasts for providing datasets that made this work possible. We also acknowledge the support of the Institute for Environmental and Climate Research and Guangdong-Hongkong-Macau Joint Laboratory of Collaborative Innovation for
395 Environmental Quality in Jinan University.

Financial support. This research was supported by the National Natural Science Foundation of China (grant number 92044302, 41805115), Guangzhou Municipal Science and Technology Project, China (grant number 202002020065), Special Fund Project for Science and Technology Innovation Strategy of Guangdong Province (grant number
400 2019B121205004), Guangdong Innovative and Entrepreneurial Research Team Program (grant number 2016ZT06N263), and National Key Research and Development Program of China (grant number 2018YFC0213906).

References

Atkinson, R.: Gas-phase tropospheric chemistry of organic compounds: a review, Atmos. Environ., 24, 1–41,
405 https://doi.org/10.1016/0960-1686(90)90438-S, 1990.

Atkinson, R., Baulch, D. L., Cox, R. A., Crowley, J. N., Hampson, R. F., Hynes, R. G., Jenkin, M. E., Rossi, M. J., Troe, J., and IUPAC Subcommittee: Evaluated kinetic and photochemical data for atmospheric chemistry: Volume II-gas phase reactions of organic species, Atmos. Chem. Phys., 6, 3625–4055, https://doi.org/10.5194/acp-6-3625-2006, 2006.

Calvert, J. G.: Test of the theory of ozone generation in Los Angeles atmosphere, Environ. Sci. Technol., 10, 248–256,
410 https://doi.org/10.1021/es60114a002, 1976.

Chang, C.-C., Yak, H.-K., and Wang, J.-L.: Consumption of hydrocarbons and its relationship with ozone formation in two Chinese megacities, Atmosphere, 11, 326, https://doi.org/10.3390/atmos11040326, 2020.

Cheng, H., Guo, H., Wang, X., Saunders, S. M., Lam, S. H., Jiang, F., Wang, T., Ding, A., Lee, S., and Ho, K. F.: On the relationship between ozone and its precursors in the Pearl River Delta: application of an observation-based model (OBM),
415 Environ. Sci. Pollut. Res., 17, 547–560, https://doi.org/10.1007/s11356-009-0247-9, 2010.

Chin, M., Jacob, D. J., Munger, J. W., Parrish, D. D., and Doddridge, B. G.: Relationship of ozone and carbon monoxide over North America, J. Geophys. Res. Atmos., 99, 14565–14573, https://doi.org/10.1029/94JD00907, 1994.

Coates, J. and Butler, T. M.: A comparison of chemical mechanisms using tagged ozone production potential (TOPP) analysis, Atmos. Chem. Phys., 15, 8795–8808, https://doi.org/10.5194/acp-15-8795–2015, 2015.

420 Daum, P. H., Kleinman, L., Imre, D. G., Nunnermacker, L. J., Lee, Y. N., Springston, S. R., Newman, L., and Weinstein-Lloyd, J.: Analysis of the processing of Nashville urban emissions on July 3 and July 18, 1995, J. Geophys. Res. Atmos., 105, 9155–9164, https://doi.org/10.1029/1999jd900997, 2000.

Department of Ecology and Environment of Guangdong Province: 2015 Report on the state of Guangdong provincial environment, 38 pp., 2016.

425 Department of Ecology and Environment of Guangdong Province: 2020 Report on the state of Guangdong provincial ecology and environment, 56 pp., 2021.

Dodge, M. C.: Combined use of modeling techniques and smog chamber data to derive ozone precursor relationships. In: Dimitriades, B. (Ed.), Proceedings of the International Conference on Photochemical Oxidant Pollution and its Control, Vol II, EPA-600/3-77-0016, US EPA, RTP, NC, 881–889, 1977.

430 Heald, C. L., Jacob, D. J., Fiore, A. M., Emmons, L. K., Gille, J. C., Deeter, M. N., Warner, J., Edwards, D. P., Crawford, J. H., Hamlin, A. J., Sachse, G. W., Browell, E. V., Avery, M. A., Vay, S. A., Westberg, D. J., Blake, D. R., Singh, H. B., Sandholm, S. T., Talbot, R. W., and Fuelberg, H. E.: Asian outflow and trans-Pacific transport of carbon monoxide and ozone pollution: An integrated satellite, aircraft, and model perspective, J. Geophys. Res. Atmos., 108, 4804, https://doi.org/10.1029/2003jd003507, 2003.

435 Hsu, Y.-K., VanCuren, T., Park, S., Jakober, C., Herner, J., FitzGibbon, M., Blake, D. R., and Parrish, D. D.: Methane emissions inventory verification in southern California, Atmos. Environ., 44, 1–7, https://doi.org/10.1016/j.atmosenv.2009.10.002, 2010.

Huang, Z., Zhong, Z., Sha, Q., Xu, Y., Zhang, Z., Wu, L., Wang, Y., Zhang, L., Cui, X., Tang, M., Shi, B., Zheng, C., Li, Z., Hu, M., Bi, L., Zheng, J., and Yan, M.: An updated model-ready emission inventory for Guangdong Province by
440 incorporating big data and mapping onto multiple chemical mechanisms, Sci. Total Environ., 769, 144535, https://doi.org/10.1016/j.scitotenv.2020.144535, 2021.

IPCC: Climate Change 2013: The Physical Science Basis. Contribution of Working Group I to the Fifth Assessment Report of the Intergovernmental Panel on Climate Change, edited by: Stocker, T. F., Qin, D., Plattner, G.-K., Tignor, M., Allen, S. K., Boschung, J., Nauels, A., Xia, Y., Bex, V., and Midgley, P. M., Cambridge University Press, Cambridge, United
445 Kingdom and New York, NY, USA, 1535 pp., 2013.

Jacob, D. J.: Introduction to Atmospheric Chemistry, Princeton University Press, Princeton, N. J., 1999.

Jiang, M., Lu, K., Su, R., Tan, Z., Wang, H., Li, L., Fu, Q., Zhai, C., Tan, Q., Yue, D., Chen, D., Wang, Z., Xie, S., Zeng, L., and Zhang, Y.: Ozone formation and key VOCs in typical Chinese city clusters, Chinese Sci. Bull., 63, 1130–1141, 2018 (in Chinese).

450 Kleinman, L. I.: The dependence of tropospheric ozone production rate on ozone precursors, Atmos. Environ., 39, 575–586, https://doi.org/10.1016/j.atmosenv.2004.08.047, 2005.

Kleinman, L. I., Daum, P. H., Lee, Y.-N., Nunnermacker, L. J., Springston, S. R., Weinstein-Lloyd, J., and Rudolph, J.: Sensitivity of ozone production rate to ozone precursors, Geophys. Res. Lett., 28, 2903–2906, https://doi.org/10.1029/2000gl012597, 2001.

455 Kleinman, L. I., Daum, P. H., Lee, Y.-N., Nunnermacker, L. J., Springston, S. R., Weinstein-Lloyd, J., and Rudolph, J.: Ozone production efficiency in an urban area, J. Geophys. Res. Atmos., 107, ACH 23-1–ACH 23-12, https://doi.org/10.1029/2002jd002529, 2002.

Kleinman, L. I., Lee, Y.-N., Springston, S. R., Nunnermacker, L., Zhou, X., Brown, R., Hallock, K., Klotz, P., Leahy, D., Lee, J. H., and Newman, L.: Ozone formation at a rural site in the southeastern United States, J. Geophys. Res. Atmos., 99,
460 3469–3482, https://doi.org/10.1029/93JD02991, 1994.

Lei, W., Zhang, R., Tie, X., and Hess, P.: Chemical characterization of ozone formation in the Houston-Galveston area: A chemical transport model study, J. Geophys. Res. Atmos., 109, https://doi.org/10.1029/2003jd004219, 2004.

Li, K., Chen, L., Ying, F., White, S. J., Jang, C., Wu, X., Gao, X., Hong, S., Shen, J., Azzi, M., and Cen, K.: Meteorological and chemical impacts on ozone formation: A case study in Hangzhou, China, Atmos. Res., 196, 40–52,
465 https://doi.org/10.1016/j.atmosres.2017.06.003, 2017.

Lin, Y., Jiang, F., Zhao, J., Zhu, G., He, X., Ma, X., Li, S., Sabel, C. E., and Wang, H.: Impacts of O_3 on premature mortality and crop yield loss across China, Atmos. Environ., 194, 41–47, https://doi.org/10.1016/j.atmosenv.2018.09.024, 2018.

Liu, J., Wu, D., Fan, S., Liao, Z., and Deng, T.: Impacts of precursors and meteorological factors on ozone pollution in Pearl River Delta, China Environ. Sci., 37, 813–820, 2017 (in Chinese).

470 Liu, S. C., Trainer, M., Fehsenfeld, F. C., Parrish, D. D., Williams, E. J., Fahey, D. W., Hübler, G., and Murphy, P. C.: Ozone production in the rural troposphere and the implications for regional and global ozone distributions, J. Geophys. Res. Atmos., 92, 4191–4207, https://doi.org/10.1029/JD092iD04p04191, 1987.

Lu, K. D., Rohrer, F., Holland, F., Fuchs, H., Bohn, B., Brauers, T., Chang, C. C., Häseler, R., Hu, M., Kita, K., Kondo, Y., Li, X., Lou, S. R., Nehr, S., Shao, M., Zeng, L. M., Wahner, A., Zhang, Y. H., and Hofzumahaus, A.: Observation and

475 modelling of OH and HO$_2$ concentrations in the Pearl River Delta 2006: a missing OH source in a VOC rich atmosphere, Atmos. Chem. Phys., 12, 1541–1569, https://doi.org/10.5194/acp-12-1541-2012, 2012.

Lu, K. D., Zhang, Y., Su, H., Brauers, T., Chou, C. C., Hofzumahaus, A., Liu, S. C., Kita, K., Kondo, Y., Shao, M., Wahner, A., Wang, J., Wang, X., and Zhu, T.: Oxidant (O$_3$+NO$_2$) production processes and formation regimes in Beijing. J. Geophys. Res. Atmos., 115, https://doi.org/10.1029/2009jd012714, 2010a.

480 Lu, K., Zhang, Y., Su, H., Shao, M., Zeng, L., Zhong, L., Xiang, Y., Chang, C. C., Chou, C. K. C., and Andreas, W.: Regional ozone pollution and key controlling factors of photochemical ozone production in Pearl River Delta during summer time, Sci. China Chem., 53, 651–663, https://doi.org/10.1007/s11426-010-0055-6, 2010b.

Mao, J., Ren, X., Chen, S., Brune, W. H., Chen, Z., Martinez, M., Harder, H., Lefer, B., Rappenglück, B., Flynn, J., and Leuchner, M.: Atmospheric oxidation capacity in the summer of Houston 2006: Comparison with summer measurements in

485 other metropolitan studies, Atmos. Environ., 44, 4107–4115, https://doi.org/10.1016/j.atmosenv.2009.01.013, 2010.

Sander, S. P., Friedl, R. R., Ravishankara, A. R., Golden, D. M., Kolb, C. E., Kurylo, M. J., Huie, R. E., Orkin, V. L., Molina, M. J., Moortgat, G. K., and Finlayson-Pitts, B. J.: Chemical Kinetics and Photochemical Data for Use in Atmospheric Studies Evaluation Number 14, JPL Publication 02-25, 2003.

Seinfeld, J. H. and Pandis, S. N.: Atmospheric Chemistry and Physics: From Air Pollution to Climate Change, John Wiley &

490 Sons, Inc., 1998.

Shao, M., Huang, D., Gu, D., Lu, S., Chang, C., and Wang, J.: Estimate of anthropogenic halocarbon emission based on measured ratio relative to CO in the Pearl River Delta region, China, Atmos. Chem. Phys., 11, 5011–5025, https://doi.org/10.5194/acp-11-5011-2011, 2011.

Shao, M., Zhang, Y., Zeng, L., Tang, X., Zhang, J., Zhong, L., and Wang, B.: Ground-level ozone in the Pearl River Delta

495 and the roles of VOC and NOx in its production, J. Environ. Manage., 90, 512–518, https://doi.org/10.1016/j.jenvman.2007.12.008, 2009.

Shiu, C.-J., Liu, S. C., Chang, C.-C., Chen, J.-P., Chou, C. C. K., Lin, C.-Y., and Young, C.-Y.: Photochemical production of ozone and control strategy for Southern Taiwan, Atmos. Environ., 41, 9324–9340, https://doi.org/10.1016/j.atmosenv.2007.09.014, 2007.

500   Sillman, S., He, D., Pippin, M. R., Daum, P. H., Imre, D. G., Kleinman, L. I., Lee, J. H., and Weinstein-Lloyd, J.: Model correlations for ozone, reactive nitrogen, and peroxides for Nashville in comparison with measurements: Implications for O_3-NOx-hydrocarbon chemistry, J. Geophys. Res. Atmos., 103, 22629–22644, https://doi.org/10.1029/98jd00349, 1998.

Sillman, S., Vautard, R., Menut, L., and Kley, D.: O_3-NOx-VOC sensitivity and NOx-VOC indicators in Paris: Results from models and atmospheric pollution over the Paris area (ESQUIF) measurements, J. Geophys. Res. Atmos., 108,
505   https://doi.org/10.1029/2002jd001561, 2003.

Singh, H. B.: Atmospheric halocarbons: evidence in favor of reduced average hydroxyl radical concentration in the troposphere, Geophys. Res. Lett., 4, 101–104, https://doi.org/10.1029/GL004i003p00101, 1977.

Song, C., Wu, L., Xie, Y., He, J., Chen, X., Wang, T., Lin, Y., Jin, T., Wang, A., Liu, Y., Dai, Q., Liu, B., Wang, Y. -N., and Mao, H.: Air pollution in China: Status and spatiotemporal variations, Environ. Pollut., 227, 334–347,
510   https://doi.org/10.1016/j.envpol.2017.04.075, 2017.

Tan, Z., Lu, K., Hofzumahaus, A., Fuchs, H., Bohn, B., Holland, F., Liu, Y., Rohrer, F., Shao, M., Sun, K., Wu, Y., Zeng, L., Zhang, Y., Zou, Q., Kiendler-Scharr, A., Wahner, A., and Zhang, Y.: Experimental budgets of OH, HO_2, and RO_2 radicals and implications for ozone formation in the Pearl River Delta in China 2014, Atmos. Chem. Phys., 19, 7129–7150, https://doi.org/10.5194/acp-19-7129-2019, 2019.

515   Tang, X., Wang, Z., Zhu, J., Gbaguidi, A. E., Wu, Q., Li, J., and Zhu, T.: Sensitivity of ozone to precursor emissions in urban Beijing with a Monte Carlo scheme, Atmos. Environ., 44, 3833–3842, https://doi.org/10.1016/j.atmosenv.2010.06.026, 2010.

Tang, X., Zhu, J., Wang, Z. F., Wang, M., Gbaguidi, A., Li, J., Shao, M., Tang, G. Q., and Ji, D. S.: Inversion of CO emissions over Beijing and its surrounding areas with ensemble Kalman filter, Atmos. Environ., 81, 676–686,
520   https://doi.org/10.1016/j.atmosenv.2013.08.051, 2013.

Thielmann, A., Prévôt, A. S., and Staehelin, J.: Sensitivity of ozone production derived from field measurements in the Italian Po basin, J. Geophys. Res. Atmos., 107, https://doi.org/10.1029/2000jd000119, 2002.

Trainer, M., Parrish, D. D., Goldan, P. D., Roberts, J., and Fehsenfeld, F. C.: Review of observation-based analysis of the regional factors influencing ozone concentrations, Atmos. Environ., 34, 2045–2061, https://doi.org/10.1016/S1352-
525   2310(99)00459-8., 2000.

Trainer, M., Ridley, B. A., Buhr, M. P., Kok, G., Walega, J., Hübler, G., Parrish, D. D., and Fehsenfeld, F. C.: Regional ozone and urban plumes in the southeastern United States: Birmingham, A case study, J. Geophys. Res. Atmos., 100, 18823–18834, https://doi.org/10.1029/95JD01641, 1995.

Wang, B., Liu, Y., Shao, M., Lu, S., Wang, M., Yuan, B., Gong, Z., He, L., Zeng, L., Hu, M., and Zhang, Y.: The
530   contributions of biomass burning to primary and secondary organics: A case study in Pearl River Delta (PRD), China, Sci. Total Environ., 569–570, 548–556, https://doi.org/10.1016/j.scitotenv.2016.06.153, 2016.

Wang, L., Liu, D., Han, G., Wang, Y., Qing, T., and Jiang, L.: Study on the relationship between surface ozone concentrations and meteorological conditions in Nanjing, China, Acta Scientiae Circumstantiae, 38, 1285–1296, 2018 (in Chinese).

535 Wang, T., Xue, L., Brimblecombe, P., Lam, Y. F., Li, L., and Zhang, L.: Ozone pollution in China: A review of concentrations, meteorological influences, chemical precursors, and effects, Sci. Total Environ., 575, 1582–1596, https://doi.org/10.1016/j.scitotenv.2016.10.081, 2017.

Wang, X., Carmichael, G., Chen, D., Tang, Y., and Wang, T.: Impacts of different emission sources on air quality during March 2001 in the Pearl River Delta (PRD) region, Atmos. Environ., 39, 5227–5241,
540 https://doi.org/10.1016/j.atmosenv.2005.04.035, 2005.

Wang, Y., Guo, H., Zou, S., Lyu, X., Ling, Z., Cheng, H., and Zeren, Y.: Surface O_3 photochemistry over the South China Sea: Application of a near-explicit chemical mechanism box model, Environ. Pollut., 234, 155–166, https://doi.org/10.1016/j.envpol.2017.11.001, 2018.

Wang, Y., Wang, H., Guo, H., Lyu, X., Cheng, H., Ling, Z., Louie, P. K. K., Simpson, I. J., Meinardi, S., and Blake, D. R.:
545 Long-term O_3-precursor relationships in Hong Kong: field observation and model simulation, Atmos. Chem. Phys., 17, 10919–10935, https://doi.org/10.5194/acp-17-10919-2017, 2017.

Wiegand, A. N. and Bofinger, N. D.: Review of empirical methods for the calculation of the diurnal NO_2 photolysis rate coefficient, Atmos. Environ., 34, 99–108, https://doi.org/10.1016/S1352-2310(99)00294-0, 2000.

Wei, X., Liu, Q., Lam, K. S., and Wang, T.: Impact of precursor levels and global warming on peak ozone concentration in
550 the Pearl River Delta region of China, Adv. Atmos. Sci., 29, 635–645, https://doi.org/10.1007/s00376-011-1167-4, 2012.

Wu, C., Wang, C., Wang, S., Wang, W., Yuan, B., Qi, J., Wang, B., Wang, H., Wang, C., Song, W., Wang, X., Hu, W., Lou, S., Ye, C., Peng, Y., Wang, Z., Huangfu, Y., Xie, Y., Zhu, M., Zheng, J., Wang, X., Jiang, B., Zhang, Z., and Shao, M.: Measurement report: Important contributions of oxygenated compounds to emissions and chemistry of volatile organic compounds in urban air, Atmospheric Chemistry and Physics, 20, 14769-14785, 10.5194/acp-20-14769-2020, 2020.

555 Xu, Z., Xue, L., Wang, T., Xia, T., Gao, Y., Louie, P. K. K., and Luk, C. W. Y.: Measurements of peroxyacetyl nitrate at a background site in the Pearl River Delta region: Production efficiency and regional transport, Aerosol Air Qual. Res., 15, 833–841, https://doi.org/10.4209/aaqr.2014.11.0275, 2015.

Xue, L., Wang, T., Wang, X., Blake, D. R., Gao, J., Nie, W., Gao, R., Gao, X., Xu, Z., Ding, A., Huang, Y., Lee, S., Chen, Y., Wang, S., Chai, F., Zhang, Q., and Wang, W.: On the use of an explicit chemical mechanism to dissect peroxy acetyl
560 nitrate formation, Environ. Pollut., 195, 39–47, https://doi.org/10.1016/j.envpol.2014.08.005, 2014.

Yang, L., Luo, H., Yuan, Z., Zheng, J., Huang, Z., Li, C., Lin, X., Louie, P. K. K., Chen, D., and Bian, Y.: Quantitative impacts of meteorology and precursor emission changes on the long-term trend of ambient ozone over the Pearl River Delta, China, and implications for ozone control strategy, Atmos. Chem. Phys., 19, 12901–12916, https://doi.org/10.5194/acp-19-12901-2019, 2019.

删除[Liu Emma]: Xue, L., Wang, T., Wang, X., Blake, D. R., Gao, J., Nie, W., Gao, R., Gao, X., Xu, Z., Ding, A., Huang, Y., Lee, S., Chen, Y., Wang, S., Chai, F., Zhang, Q., and Wang, W.: On the use of an explicit chemical mechanism to dissect peroxy acetyl nitrate formation, Environ. Pollut., 195, 39–47, https://doi.org/10.1016/j.envpol.2014.08.005, 2014.

565 Yang, Y., Shao, M., Keβel, S., Li, Y., Lu, K., Lu, S., Williams, J., Zhang, Y., Zeng, L., Nölscher, A. C., Wu, Y., Wang, X., and Zheng, J.: How the OH reactivity affects the ozone production efficiency: case studies in Beijing and Heshan, China, Atmos. Chem. Phys., 17, 7127–7142, https://doi.org/10.5194/acp-17-7127-2017, 2017.

Yao, B., Vollmer, M. K., Zhou, L. X., Henne, S., Reimann, S., Li, P. C., Wenger, A., and Hill, M.: In-situ measurements of atmospheric hydrofluorocarbons (HFCs) and perfluorocarbons (PFCs) at the Shangdianzi regional background station, China,
570 Atmos. Chem. Phys., 12, 10181–10193, https://doi.org/10.5194/acp-12-10181-2012, 2012.

Yarwood, G., Rao, S., Yocke, M., and Whitten, G.: Updates to the Carbon Bond Chemical Mechanism: CB05. Technical Report, Final Report to US EPA, RT-0400675, 2005.

Yu, D., Tan, Z., Lu, K., Ma, X., Li, X., Chen, S., Zhu, B., Lin, L., Li, Y., Qiu, P., Yang, X., Liu, Y., Wang, H., He, L., Huang, X., and Zhang, Y.: An explicit study of local ozone budget and NOx-VOCs sensitivity in Shenzhen China, Atmos.
575 Environ., 224, 117304, https://doi.org/10.1016/j.atmosenv.2020.117304, 2020.

Zaveri, R. A., Berkowitz, C. M., Kleinman, L. I., Springtson, S. R. Doskey, P. V., Lonneman, W. A., and Spicer, C. W.: Ozone production efficiency and NOx depletion in an urban plume: Interpretation of field observations and implications for evaluating O₃-NOx-VOC sensitivity, J. Geophys. Res. Atmos., 108, https://doi.org/10.1029/2002jd003144, 2003.

Zhang, Q., Yuan, B., Shao, M., Wang, X., Lu, S., Lu, K., Wang, M., Chen, L., Chang, C. C., and Liu, S. C.: Variations of
580 ground-level O3 and its precursors in Beijing in summertime between 2005 and 2011, Atmos. Chem. Phys., 14, 6089–6101, https://doi.org/10.5194/acp-14-6089-2014, 2014.

Zhang, Y. H., Su, H., Zhong, L. J., Cheng, Y. F., Zeng, L. M., Wang, X. S., Xiang, Y. R., Wang, J. L., Gao, D. F., Shao, M., Fan, S. J., and Liu, S. C.: Regional ozone pollution and observation-based approach for analyzing ozone–precursor relationship during the PRIDE-PRD2004 campaign, Atmos. Environ., 42, 6203–6218,
585 https://doi.org/10.1016/j.atmosenv.2008.05.002, 2008.

Zhang, Y. N., Xiang, Y. R., Chan, L. Y., Chan, C. Y., Sang, X. F., Wang, R., and Fu, H. X.: Procuring the regional urbanization and industrialization effect on ozone pollution in Pearl River Delta of Guangdong, China, Atmos. Environ., 45, 4898–4906, https://doi.org/10.1016/j.atmosenv.2011.06.013, 2011.

Zhao, W., Tang, G., Yu, H., Yang, Y., Wang, Y., Wang, L., An, J., Gao, W., Hu, B., Cheng, M., An, X., Li, X., and Wang,
590 Y.: Evolution of boundary layer ozone in Shijiazhuang, a suburban site on the North China Plain, J. Environ. Sci., 83, 152–160, https://doi.org/10.1016/j.jes.2019.02.016, 2019.
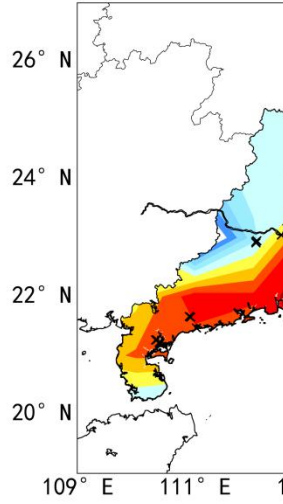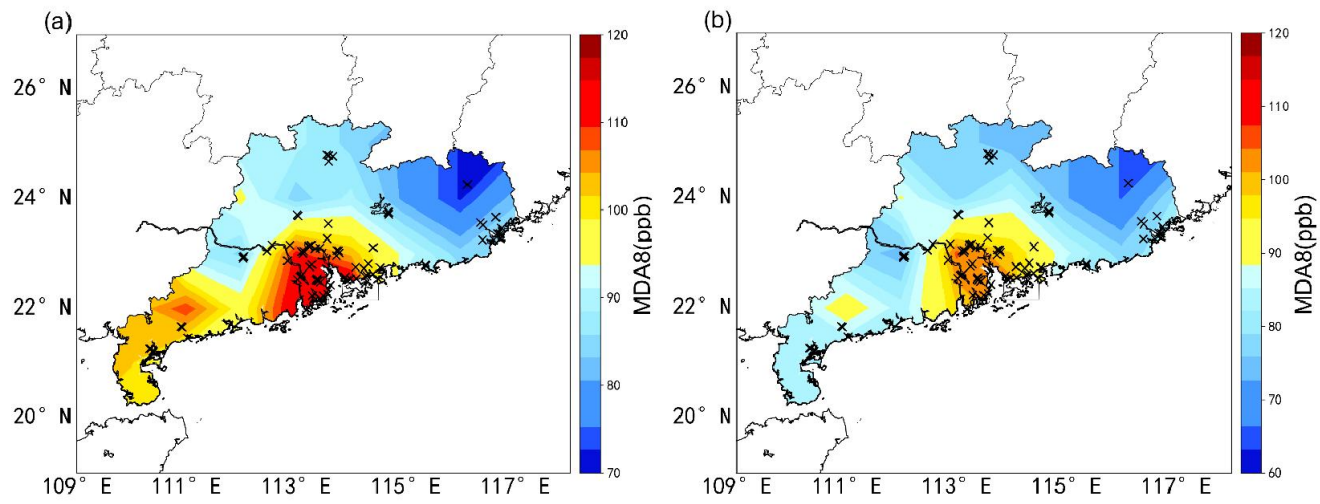
Figure 1: (a) Spatial distribution of the average maximum daily 8-hour average ozone concentration (MDA8) in Guangdong during the study period, black crosses mark the locations of observation sites. (b) Same as (a) but for MDA8 of all ozone exceeding days in Guangdong in 2018 and 2019.

595
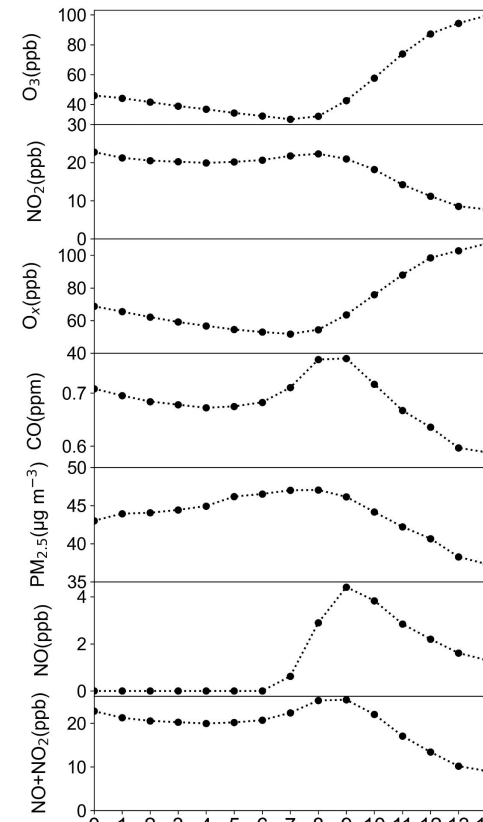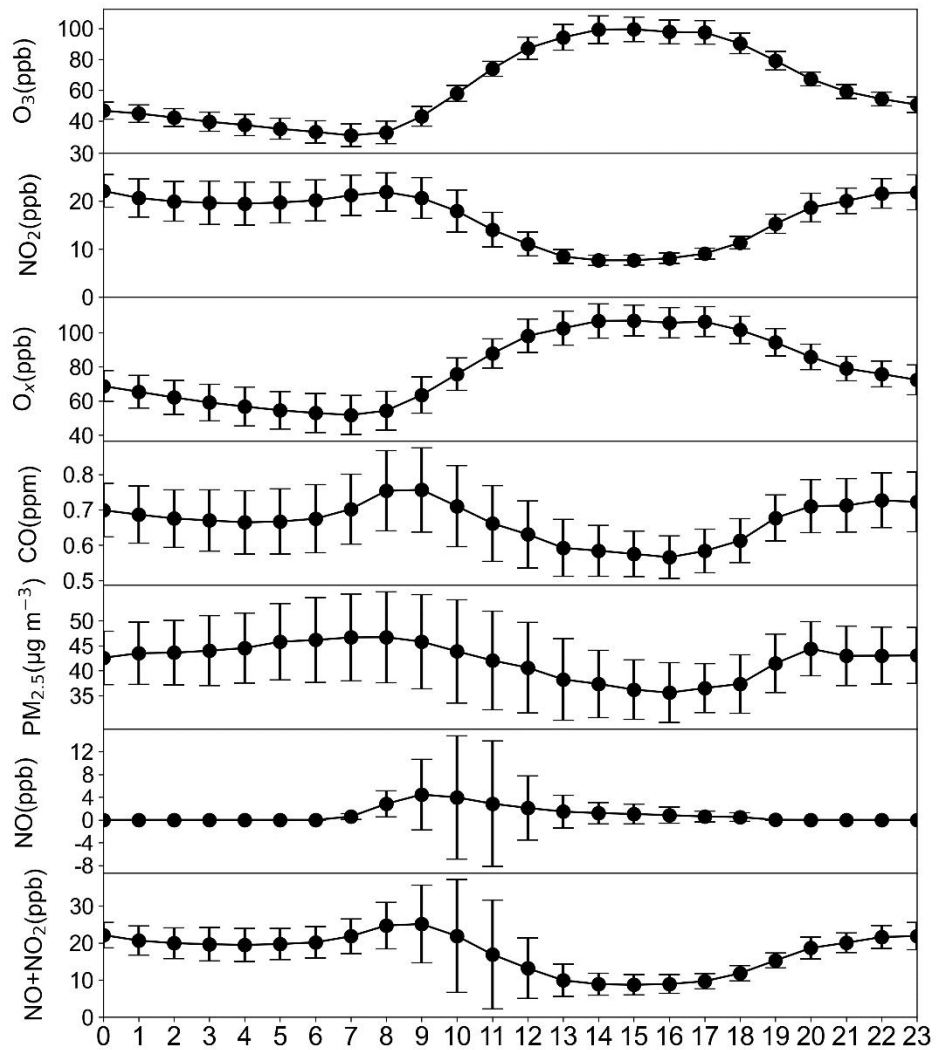
Figure 2: Average diurnal variations of air pollutants, O₃, NO₂, Oₓ, CO, PM₂.₅, NO and NO+NO₂, observed at the 77 stations in Guangdong during the two episodes.
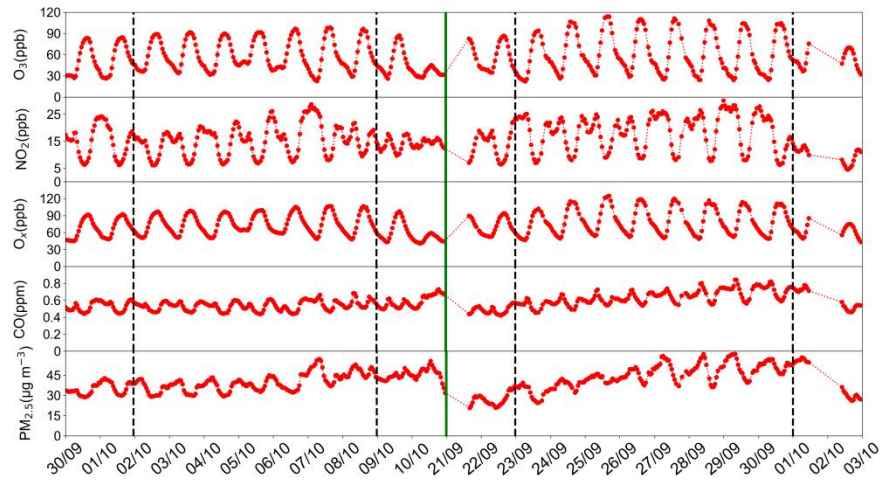
600 **Figure 3: Hourly surface concentrations of air pollutants during the study period. The green line is added to separate the two episodes, the black dashed lines indicate two days before and two days after the episodes.**

删除[fang]: **the**

删除[Liu Emma]:

Figure 4: Same as Fig. 3 except for meteorological parameters.

Figure 4: Hourly average OH concentrations between 08:00 and 13:00 derived from the OBM are shown in black line with black dots; observed OH concentrations by Tan et al. (2019) are shown in blue line and blue shade; calculated OH concentrations by Wang et al. (2018) are shown in red line and red shade. The blue shade denotes the 25% and 75% percentiles of the data, the red shade indicates the 95% C. I. of the data. The red cross with red vertical whiskers denotes the mean OH concentration and 1-standard deviation, respectively, calculated by a box model constrained by observed ambient conditions during the two episodes.

605

删除[Liu Emma]: **5**

删除[fang]: **,**

删除[fang]: **,**

删除[fang]: **observed**
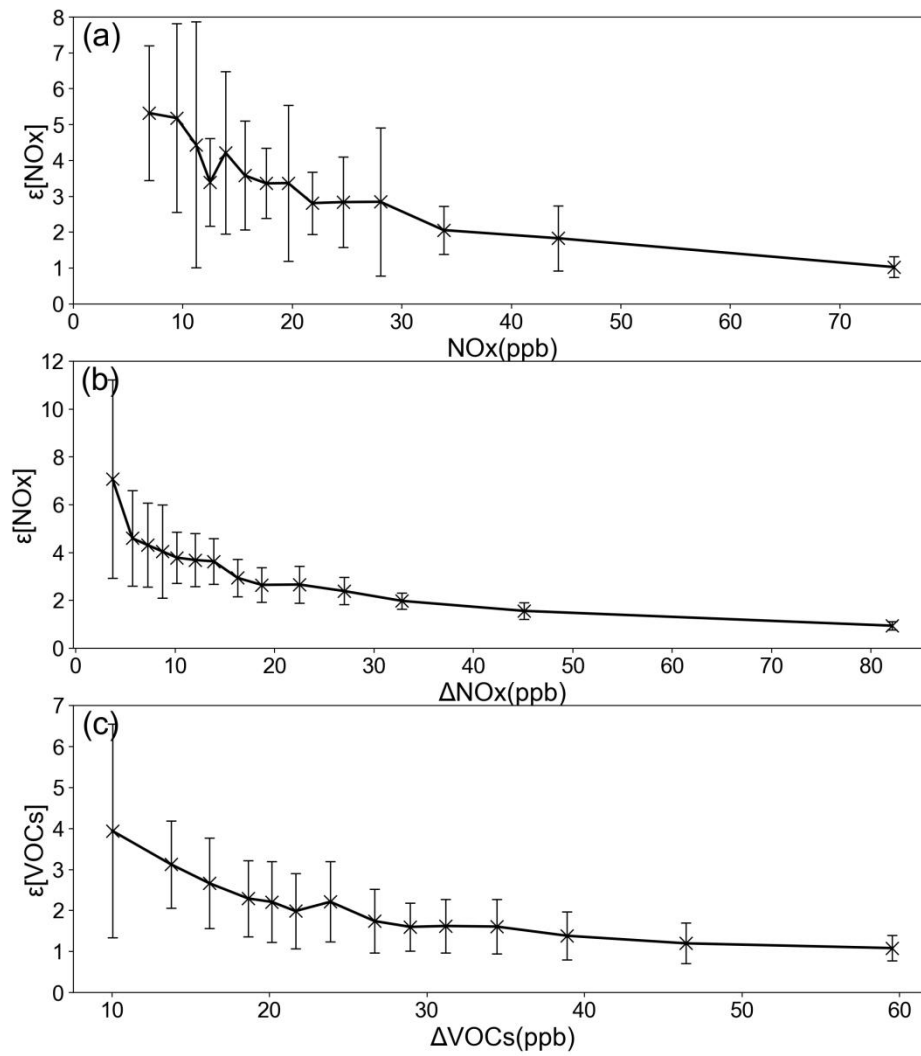
Figure 5: Ozone production efficiency plotted as a function of NO$_x$ (a), oxidized NO$_x$ (b), and oxidized VOC (c).

设置格式[liuru]: 两端对齐

删除[Liu Emma]: 6

610
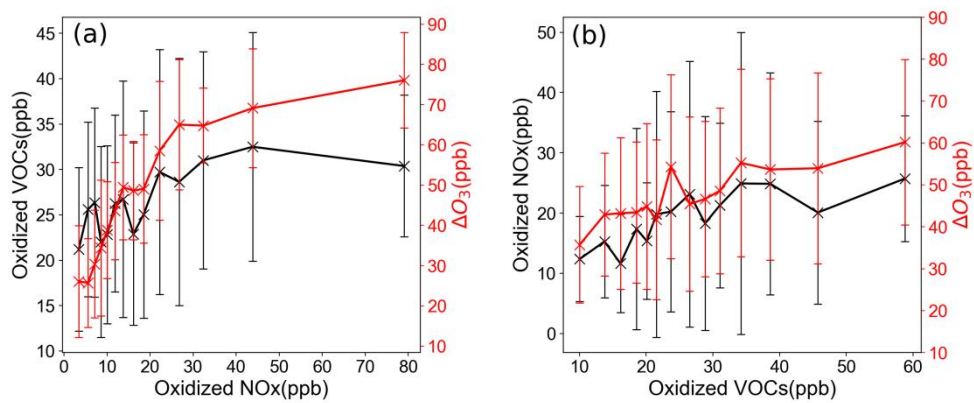
Figure 6: Ozone formation rate (ΔO_3, right hand side in red) and the oxidized VOC (left hand side in black) plotted as a function of oxidized NO$_x$ (a). Ozone formation rate (ΔO_3, right hand side in red) and oxidized NO$_x$ (left hand side in black) plotted as a function of the oxidized VOC (b).

删除[Liu Emma]: **7**

$$[\Delta O_3] = 0.755 \times [\Delta NOx] + 0.24$$
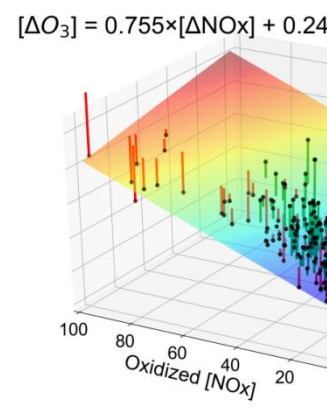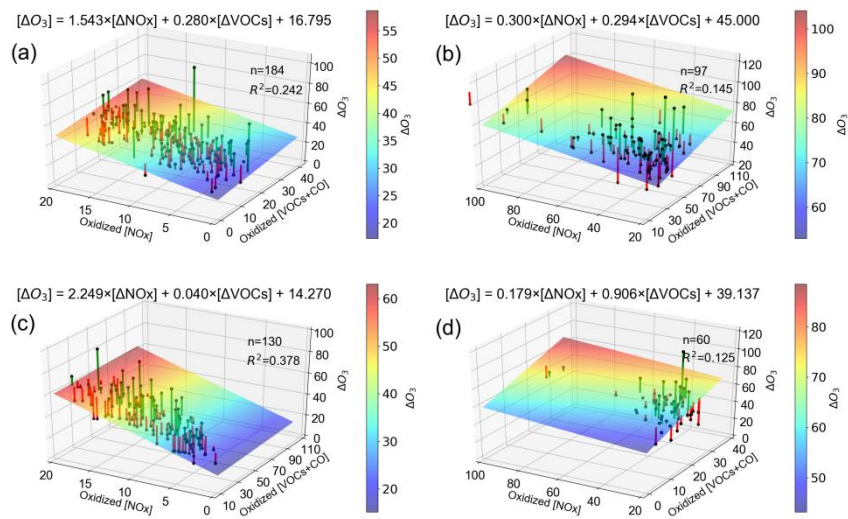
Figure 7: Three-dimensional depiction of ozone formation rate (ΔO3, z-axis) plotted as a function of oxidized NOx (x-axis) and oxidized VOC (y-axis). The black dots denote values of ΔO3, the colored plane is the best linear fit to the black dots, and the green and red bars denote positive and negative deviations from the plane, respectively. The equation listed represents the surface as a function of oxidized NOx and oxidized VOC. R2 is the square of correlation coefficient of the linear regression. Four quadrants: (a) low NOx and low VOC (NOx<20 ppb, VOC<25 ppb), (b) high NOx and high VOC (NOx>20 ppb, VOC>25 ppb), (c) low NOx and high VOC (NOx<20 ppb, VOC>25 ppb), (d) high NOx and low VOC (NOx>20 ppb, VOC<25 ppb).

删除[Liu Emma]:

Figure 8: Three-dimensional depiction of ozone formation rate (ΔO₃, z-axis) plotted as a function of oxidized NOₓ (x-axis) and oxidized VOC (y-axis). The black dots denote values of ΔO₃, the colored plane is the best linear fit to the black dots, and the green and red bars denote positive and negative deviations from the plane, respectively. The equation listed represents the surface as a function of oxidized NOₓ and oxidized VOC. R² is the square of correlation coefficient of the linear regression.

设置格式[Liu Emma]: 两端对齐

删除[Liu Emma]: **9**

删除[liuru]: **Same as Fig. 8 except divided into four quadrants: (a) low NOₓ and low VOC (NOₓ<20 ppb, VOC<25 ppb), (b) high NOₓ and high VOC (NOₓ>20 ppb, VOC>25 ppb), (c) low NOₓ and high VOC (NOₓ<20 ppb, VOC>25 ppb), (d) high NOₓ and low VOC (NOₓ>20 ppb, VOC<25 ppb).**
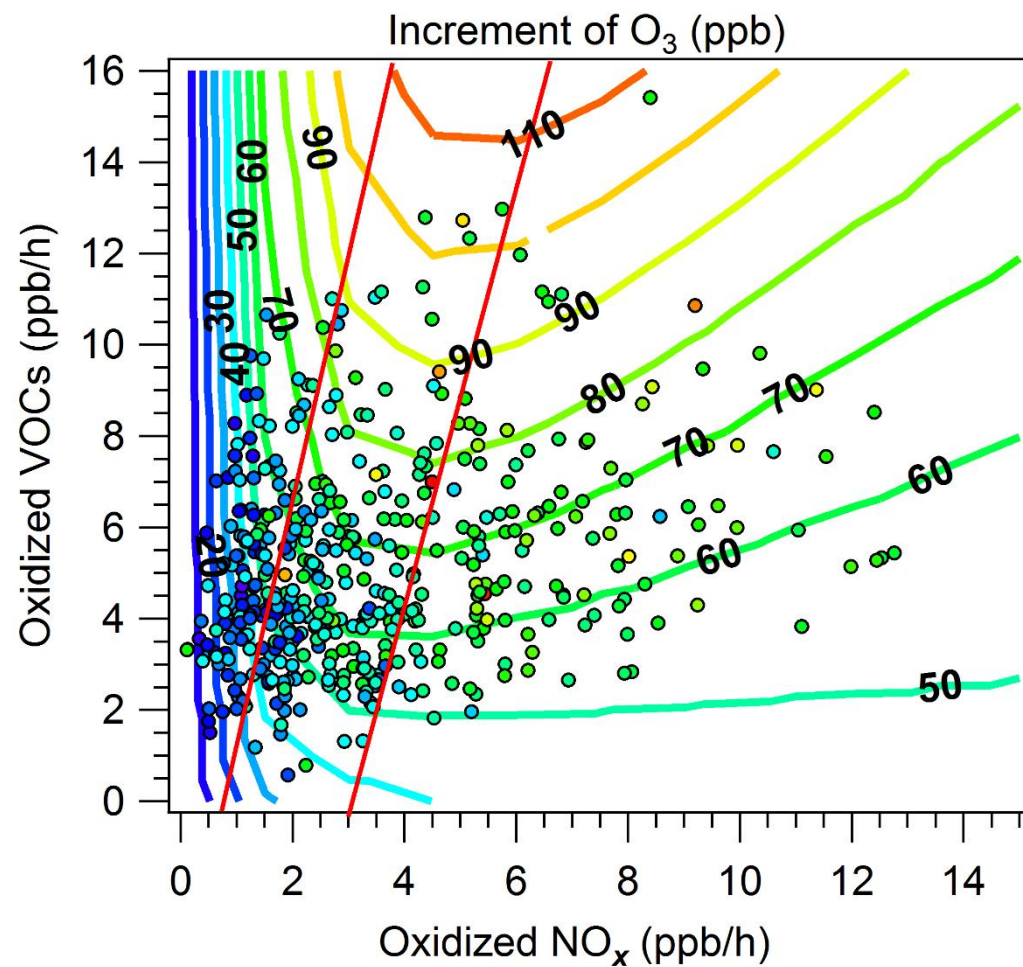
Figure 8: Ozone isopleths (in ppbv) of traditional 2D-EKMA plot for the two episodes calculated by the box model are shown in colored lines, ozone concentrations at 13:00 local time derived by the OBM are shown in colored dots, x-axis and y-axis are hourly oxidized NO_x and oxidized VOC, respectively.